Special Section: Coupled Surface–Subsurface Modeling
Vadose Zone Journal

# Comparison of Data Assimilation Techniques for a Coupled Model of Surface and Subsurface Flow

Matteo Camporese,* Claudio Paniconi, Mario Putti, and Paolo Salandin

Data assimilation in the geophysical sciences refers to methodologies to optimally merge model predictions and observations. The ensemble Kalman filter (EnKF) is a statistical sequential data assimilation technique explicitly developed for nonlinear filtering problems. It is based on a Monte Carlo approach that approximates the conditional probability densities of the variables of interest by a finite number of randomly generated model trajectories. In Newtonian relaxation or nudging (NN), which can be viewed as a special case of the classic Kalman filter, model variables are driven toward observations by adding to the model equations a forcing term, or relaxation component, that is proportional to the difference between simulation and observation. The forcing term contains four-dimensional weighting functions that can, ideally, incorporate prior knowledge about the characteristic scales of spatial and temporal variability of the state variable(s) being assimilated. In this study, we examined the EnKF and NN algorithms as implemented for a complex hydrologic model that simulates catchment dynamics, coupling a three-dimensional finite element Richards' equation solver for variably saturated porous media and a finite difference diffusion wave approximation for surface water flow. We report on the retrieval performance of the two assimilation schemes for a small catchment in Belgium. The results of the comparison show that nudging, while more straightforward and less expensive computationally, is not as effective as the ensemble Kalman filter in retrieving the true system state. We discuss some of the strengths and weaknesses, both physical and numerical, of the NN and EnKF schemes.

Abbreviations: DEM, digital elevation model; EnKF, ensemble Kalman filter; NN, Newtonian nudging.

Catchment dynamics are strongly influenced by subsurface processes. Spatio-temporal distributions of soil moisture in the vadose zone affect the hydrologic cycle and play a key role in agriculture and meteorology (e.g., Georgakakos, 1996; Rodríguez-Iturbe et al., 1999; Reichle et al., 2002a). Surface soil moisture is a crucial storage parameter and controls the partitioning of energy and mass in evapotranspiration and rainfall–runoff processes (e.g., Vereecken et al., 2008). The saturated zone also plays an important role in determining a catchment response to atmospheric forcing. Recent experimental evidence (Kosugi et al., 2008) has shown that groundwater flow is responsible for most of the observed streamflow in a headwater catchment, while Wörman et al. (2007) and Kollet and Maxwell (2008a,b) demonstrated the important contribution of subsurface processes to the formation of streamflow in large-scale catchments. Depending on the catchment, other factors besides subsurface soil and geologic features (e.g., topography and vegetation) will, of course, also be important. Modeling tools capable of simulating the fully three-dimensional dynamics of the groundwater–surface water flow system are of paramount importance for fully capturing the hydrologic behavior of catchments. Recently, several models for the distributed, process-based simulation of coupled surface and subsurface flow have been developed (e.g., VanderKwaak and Sudicky, 2000; Morita and Yen, 2002; Panday and Huyakorn, 2004; Kollet and Maxwell, 2006; Qu and Duffy, 2007; Weill et al., 2009; Camporese et al., 2009a). These models allow an accurate description of critical hydrologic processes such as rainfall–runoff–infiltration partitioning, soil moisture redistribution, groundwater recharge, and stream–aquifer interactions. Nevertheless, uncertainties and inaccuracies in model structure, parameter estimates, and boundary conditions induce errors in the model predictions. Data assimilation, which allows the merging of information from spatially and temporally distributed observations and simulations, is an effective technique to improve accuracy and quantify uncertainties of model predictions (McLaughlin, 2002).

Several data assimilation studies have been conducted recently based on process-based hydrologic models (Margulis et al., 2006). The classic Kalman filter (KF) (Kalman, 1960) is a Bayesian method that yields the best linear unbiased estimate of a measurement update for linear dynamics if the noise (error) can be characterized as a Gaussian process. As such, it is suitable for saturated groundwater flow problems and has been used, for example, to reduce the

M. Camporese and P. Salandin, Dipartimento di Ingegneria Idraulica, Marittima, Ambientale e Geotecnica, Università degli Studi di Padova, Italy; C. Paniconi, Institut National de la Recherche Scientifique– Centre Eau, Terre et Environnement, Université du Québec, Canada; M. Putti, Dipartimento di Metodi e Modelli Matematici per le Scienze Applicate, Università degli Studi di Padova, Italy.
*Corresponding author (camporese@idra.unipd.it).

Vadose Zone J. 8:837–845
doi:10.2136/vzj2009.0018
Received 28 Feb. 2009.
Published online 9 Oct. 2009.

uncertainty in parameter estimation (Hantush and Mariño, 1997). For nonlinear dynamics, the extended Kalman filter (EKF) has been developed by linearizing the system equations along a reference state trajectory based on the previous estimate. Entekhabi et al. (1994) and Hoeben and Troch (2000) demonstrated the potential of EKF for estimating soil moisture profiles using sequential assimilation of remotely sensed surface moisture data in a one-dimensional modeling context. Walker et al. (2001) compared direct insertion (a simple data assimilation technique) and the EKF using synthetic data, concluding that the Kalman filter-based assimilation scheme is superior to the direct insertion method. The better performance of the Kalman filter is a consequence of its ability to adjust the entire soil moisture vertical profile, while direct insertion can only alter the profile within the observation depth.

Both the KF and the EKF define an explicit model for the propagation in time of the covariance matrices expressing system noise statistics. The evaluation of these covariance matrices is nontrivial, as demonstrated, for instance, by Van Geer et al. (1991) and Drécourt et al. (2006b). Moreover, due to computational and stability limitations (Reichle et al., 2002a), the KF and EKF are impractical for large, highly nonlinear, three-dimensional models (Evensen, 2006). Data assimilation studies applied to surface–subsurface simulators have thus been limited to simpler schemes such as NN, as proposed by Davies and Turner (1977) and subsequently applied in limited-area and regional climate modeling (e.g., Stauffer and Seaman, 1994; Waldron et al., 1996; von Storch et al., 2000; Miguez-Macho et al., 2004). In hydrology, NN has been implemented for a TOPMODEL-based soil–vegetation–atmosphere transfer model (Houser et al., 1998; Pauwels et al., 2001) and for a detailed Richards' equation-based model (Paniconi et al., 2003). A different technique applicable to large-scale nonlinear problems is the EnKF. The EnKF uses a Monte Carlo approach to generate an ensemble of model trajectories from which the necessary error covariances are estimated at the time of an update (Evensen, 1994). Hydrologic models that have used the EnKF include the one-dimensional Richards' equation (Das and Mohanty, 2006), three-dimensional saturated groundwater flow (Chen and Zhang, 2006) and transport (Liu et al., 2008), an integral-balance saturated–unsaturated subsurface model (Shu et al., 2005), and conceptual rainfall–runoff models (Aubert et al., 2003; Weerts and El Serafy, 2006; Clark et al., 2008).

Data assimilation is widely used in conjunction with land surface models. Several studies in this area have been published recently, addressing issues such as the sensitivity of the EnKF to ensemble size (Reichle et al., 2002a), the comparative performance of the EnKF and EKF (Reichle et al., 2002b) and of one- and two-dimensional implementations of the EnKF (Reichle and Koster, 2003), the impact of observation frequency (Walker and Houser, 2001) and of model bias (De Lannoy et al., 2007), and the potential benefit of assimilating streamflow (Pauwels and De Lannoy, 2006) and both soil moisture and streamflow (Crow and Van Loon, 2006). Land surface models (e.g., Chen et al., 1996; Liang et al., 1996; Koster and Suarez, 1996; Dai et al., 2003) typically include a thin surface soil layer coupled to one or several thicker root zone layers; they use simplified representations of lateral subsurface flow and they neglect deeper groundwater flow. To improve the simulation of catchment dynamics, there is a need for robust assimilation of measurement information, both from remote sensing and local observations, into more complex, coupled surface–subsurface models (Camporese et al., 2009b).

In this study, we compare the performance of NN and the EnKF in assimilating synthetic observations for a detailed process-based model of coupled surface– subsurface flow. The capabilities of the two assimilation techniques to retrieve the correct watershed response are assessed, and the tradeoffs between the two approaches are addressed. The simulations were conducted for the Brisy catchment, a small watershed in southeast Belgium. Realistic precipitation and evaporation data were used to set up a synthetic true simulation, from which the measurements were extracted. Groundwater pressure head, soil moisture, and streamflow observations were then assimilated for a scenario of perturbed atmospheric boundary conditions.

## Methods

### Coupled Hydrologic Model

The CATHY (CATchment HYdrology) model (Camporese et al., 2009a) couples a three-dimensional finite element Richards' equation solver to a one-dimensional digital elevation model (DEM)-based finite difference equation for surface water dynamics. The mathematical model can be written as (Bixio et al., 2000; Putti and Paniconi, 2004; Camporese et al., 2009a)

$$S_w S_s \frac{\partial \psi}{\partial t} + \phi \frac{\partial S_w}{\partial t} = \nabla \cdot \left[ K_s K_{rw} \left( S_w \right) \left( \nabla \psi + \eta_z \right) \right] + q_{ss} \left( d_w \right) \quad [1]$$

$$\frac{\partial Q}{\partial t} + c_k \frac{\partial Q}{\partial s} = D_h \frac{\partial^2 Q}{\partial s^2} + c_k q_s \left( d_w, \psi \right) \quad [2]$$

where $S_w = \theta / \phi$ is water saturation, $\theta$ is the volumetric moisture content ($m^3\ m^{-3}$), $\phi$ is porosity or saturated moisture content ($m^3\ m^{-3}$), $S_s$ is the aquifer specific storage coefficient ($m^{-1}$), $\psi$ is pressure head (m), $t$ is time (h), $K_s$ is the saturated hydraulic conductivity ($m\ h^{-1}$), $K_{rw}$ is the relative hydraulic conductivity, $\boldsymbol{\eta}_z = (0,0,1)^T$ is the unit vector in the $z$ direction, with $z$ (m) the vertical coordinate directed upward, $q_{ss}$ ($m^3\ m^{-3}\ h^{-1}$) represents distributed sources and sinks from the surface to the subsurface, $d_w$ (m) is the ponding head (depth of water on the surface of each cell), $s$ (m) is the hillslope and channel link coordinate describing the one-dimensional surface routing network, $Q$ ($m^3\ h^{-1}$) is the discharge along $s$, $c_k$ is the kinematic wave celerity ($m\ h^{-1}$), $D_h$ is the hydraulic diffusivity ($m^2\ h^{-1}$), and $q_s$ is the overland flow rate ($m^3\ m^{-1}\ h^{-1}$) as computed by the subsurface module and passed on to the surface.

The strong nonlinearities in the model arise from the unsaturated soil hydraulic functions and from the dependence of $q_s$ and $q_{ss}$ on ponding head. Spatial discretization proceeds from a DEM representing the catchment surface. These DEM cells are triangulated and replicated vertically to form a three-dimensional tetrahedral grid for the underlying soil and aquifer. Precipitation fluxes during storm events and potential evaporation during interstorm periods are the main driving forces of the model. The catchment partitions this atmospheric forcing into surface runoff, infiltration, actual evaporation, and changes in storage via a surface boundary condition switching algorithm (Putti and Paniconi, 2004). Surface saturation or ponding can occur via the infiltration excess or saturation excess mechanisms, and both of these are automatically accounted for by the same switching algorithm. Overland flow is assumed to concentrate in rills or rivulets confined to "hillslope" cells (upstream drainage area $A$ below some prescribed threshold $A^*$), while channel flow

occurs on "stream" cells ($A \geq A^*$) (Montgomery and Foufoula-Georgiou, 1993). The subsurface Eq. [1] is solved by the finite element method (Paniconi and Putti, 1994), whereas an explicit time discretization based on the Muskingum–Cunge scheme is used for the overland flow Eq. [2] (Orlandini and Rosso, 1996).

Parameters for the model include digital terrain data, surface flow characteristics such as Manning coefficients for hillslopes and channels, subsurface properties such as saturated conductivity and soil retention curves, and atmospheric forcing terms (precipitation and potential evaporation). The model-computed state variables include spatially distributed quantities (e.g., moisture content, surface and subsurface flow velocities, aquifer water levels, and ponding heads) and integral quantities (e.g., streamflow at the catchment outlet and groundwater volume). The time integration step size is dynamically adapted to ensure convergence of the nonlinear solver (D'Haese et al., 2007). Further details on the characteristics of the CATHY model are given in Camporese et al. (2009a).

## Data Assimilation Schemes

### Nudging

In Newtonian nudging, which can be viewed as a special case of a Kalman filter (Li and Navon, 2001), state variables are driven toward observations by adding to the model equation a forcing term proportional to the difference between the actual solution and the observation to be assimilated (Davies and Turner, 1977; Stauffer and Seaman, 1994). In our implementation, the forcing term is added only to Eq. [1], resulting in the following expression (Paniconi et al., 2003):

$$S_w S_s \frac{\partial \psi}{\partial t} + \phi \frac{\partial S_w}{\partial t} = \nabla \cdot \left[ K_s K_{rw} \left( \nabla \psi + \eta_z \right) \right] + q_{ss} + G \frac{\sum_{k=1}^{N_T} \sum_{l=1}^{N_X} W_{kl}^2 (\mathbf{x},t) \varepsilon_l \left[ \zeta_{o_{kl}} - \zeta_l(t) \right]}{\sum_{k=1}^{N_T} \sum_{l=1}^{N_X} W_{kl} (\mathbf{x},t)} \quad [3]$$

where $\mathbf{x} = (x,y,z)^T$ is the Cartesian spatial coordinate vector, $N_T$ and $N_X$ are the number of observation times and points, respectively, $\zeta_{okl}$ and $\zeta_l$ are the observed and computed values of the state variable being assimilated (their difference is termed the *innovation vector*), $G$ determines the relative strength of the nudging term with respect to the physical forcing function, $W_{kl}(\mathbf{x},t)$ are interpolation weights to be specified as functions of space and time, and $\varepsilon_l \leq 1$ is a factor that reflects the accuracy of the observations (equal to 1 for perfect measurements). The state variable being measured and assimilated, $\zeta$, can represent soil moisture $\theta$ or pressure head $\psi$ (positive in the saturated zone, or negative, representing suction, in the vadose zone). The units of $G$ depend on the state variable under consideration: ($h^{-1}$) when assimilating soil moisture and ($m^{-1}\ h^{-1}$) when assimilating pressure head. The weighting functions are used to spatially and temporally interpolate the innovations and can also be used to incorporate prior knowledge about the variability and characteristic scales of the state variables being assimilated (Paniconi et al., 2003). To mimic spatial and temporal correlation, Gaussian and exponential functions are used to define the weight $W_{kl}(\mathbf{x},t) = W_{xy,l} W_{z,l} W_{t,k}$ using the following expressions (Fig. 1):

$$W_{xy,l} = \exp\left[ -\left( \frac{d_l}{R_{xy}} \right)^2 \right] \quad [4a]$$

$$W_{z,l} = \exp\left[ -\left( \frac{z - z_l}{R_z} \right)^2 \right] \quad [4b]$$

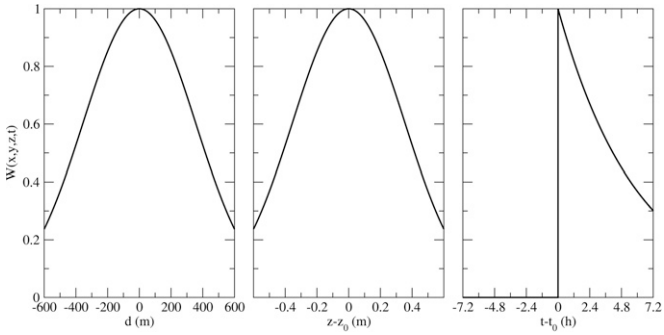


FIG. 1. The horizontal ($d$), vertical ($z - z_0$), and time ($t - t_0$) components of the Gaussian-exponential nudging four-dimensional weighting functions [$W(x,y,z,t)$] used in the Newtonian nudging runs.

$$W_{t,k} = \begin{cases} \exp\left( -\dfrac{t - t_k}{\tau_c} \right) & t \geq t_k \\ 0 & t < t_k \end{cases} \quad [4c]$$

where $d_l^2 = (x - x_l)^2 + (y - y_l)^2$, $(x_l, y_l, z_l)^T$, and $(x,y,z)^T$ are the spatial coordinates of the observation points and grid points, respectively, $R_{xy}$ and $R_z$ are the horizontal and vertical radii of influence, respectively, $t_k$ is the time of the observation, and $\tau_c$ is a characteristic measure of the observation-influenced time window.

### Ensemble Kalman Filter

The implementation of the EnKF in CATHY can be represented, as is commonly done, by three vector-valued discrete-time equations: the model equation, the measurement equation, and the update equation (Camporese et al., 2009b):

$$\mathbf{y}(t) = A\left[ \mathbf{y}(\tau), \boldsymbol{\alpha}, \mathbf{u}(t), t, \tau \right] \quad t > \tau \geq 0 \ ; \ \mathbf{y}(0) = \mathbf{y}_0(\boldsymbol{\alpha}) \quad [5]$$

$$\mathbf{z}_i = M_i \left( \mathbf{y}, \omega_i, t_i \right) \ ; \quad i = 1, \ldots, I \quad [6]$$

$$\mathbf{y}^j (t_{i+1} \mid Z_{i+1}) = \mathbf{y}^j (t_{i+1} \mid Z_i) + K_{i+1} \left\{ \mathbf{z}_{i+1} + \omega_{i+1}^j - M\left[ \mathbf{y}^j (t_{i+1} \mid Z_i) \right] \right\} \quad [7]$$

The vectors $\mathbf{y}^j(t)$, where the index $j$ indicates a single realization of the ensemble, contain the uncertain hydrologic states that in our implementation are pressure head at each node of the subsurface grid and inflow and outflow discharge at each cell of the surface discretization. The vector $\alpha$ represents the time-invariant set of soil parameters (saturated hydraulic conductivity, specific storage, porosity, retention curve parameters, etc.), while vector $\mathbf{u}(t)$ represents the time-dependent atmospheric forcing variables. The initial condition is given by $\mathbf{y}_0(\boldsymbol{\alpha})$ and the nonlinear operator $A$ describes how the state at a previous time $\tau$ is related to the state at time $t$. The operator $M$ represents the transfer model that describes how the observations are related to the system states, vector $\mathbf{z}_i$ contains the measurements obtained at time $t_i$, and $\omega_i$ is a random noise term that accounts for measurement errors. With this implementation it is possible to assimilate soil moisture, pressure head, and streamflow, either individually or together. The Kalman gain $K_{i+1}$ in Eq. [7] depends on the system state and the measurement error covariance matrices (see, e.g., Margulis et al., 2002). Each member of the ensemble is generated by perturbing the nominal

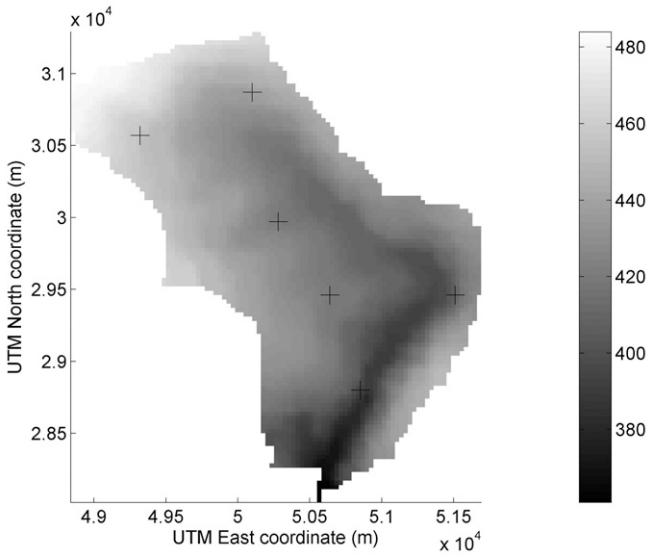


FIG. 2. A 30- by 30-m$^2$ resolution digital elevation map of the Brisy catchment. Elevation values are in meters above sea level. Crosses indicate the observation points for the data assimilation experiments.

mean values of soil parameters, initial conditions, and atmospheric forcing with random fluctuations extracted from a chosen probability density function, typically normally or lognormally distributed. The same procedure holds for the generation of the measurement ensemble. All the perturbations are spatially uncorrelated. For the time-variable atmospheric forcing fluctuations, a time correlation function is taken into account as described in Evensen (2003):

$$q_k = \gamma q_{k-1} + \sqrt{1-\gamma^2}\, w_{k-1} \quad [8]$$

where $q_k$ is the sequence of perturbations to be applied to the atmospheric boundary conditions and $w_k$ is a sequence of white noise drawn from the desired normal or lognormal distribution. The coefficient $\gamma$ determines the time decorrelation of the stochastic forcing and is computed as $1 - \Delta t/T$, where $\Delta t$ is the current time step and $T$ is the specified time decorrelation length. Note that $T$ and the aforementioned nudging parameter $\tau_c$ have different meanings: the first represents a time decorrelation length for the atmospheric boundary condition perturbations, while the second corresponds to the time decorrelation length of the nudging observations. We note that if the decorrelation time $T$ is smaller than the time between observations, $q_k$ and $q_{k-1}$ are uncorrelated and thus the EnKF can be applied.

Further details of the EnKF implementation in the CATHY model are given in Camporese et al. (2009b). It should be noted that there are other EnKF formulations, some of which account for possible bias in the model (e.g., Drécourt et al., 2006a; Kollat et al., 2008). These are promising approaches but have thus far only been used with simple groundwater models.

## Results and Discussion

### Simulation Setup

The Brisy catchment is located in the southeast of Belgium and has a drainage area of 4.64 km$^2$. The maximum length is 2.85 km from east to west and 3.27 km from north to south. The catchment contains shallow slopes in the north and steeper slopes in the south, toward the outlet (Fig. 2). The land use consists mostly of pasture and agriculture, except for a few forested areas and one urban area (the town of Brisy). A 30- by 30-m$^2$ resolution DEM was used as a basis for the hydrologic model discretization and an average soil depth of 3.0 m was assumed on the basis of topographic and soil maps. The soil profile was divided into a coarse-textured top layer (1.02 m) and a finer bottom layer (1.98 m), with each of these layers discretized into three numerical grid layers for the model (Table 1) (Hurkmans et al., 2006).

Initial conditions, boundary conditions, and model parameters are all possible sources of error for the model. In this analysis, we considered a set of atmospheric boundary conditions biased with respect to a "true" (or "base") run, to assess the capability of the NN and EnKF data assimilation schemes to retrieve the true state for a number of scenarios of a relatively long simulation (3600 h, i.e., 150 d). In these scenarios, the variables being assimilated were surface soil moisture ($\theta$), pressure head at the bottom layer of the catchment ($\psi$), and, only for the EnKF, streamflow at the catchment outlet ($Q$). First, a "base run" or "true" simulation was performed to generate observed data synthetically, using atmospheric boundary conditions corresponding to a 150-d storm–interstorm period for the Brisy catchment between February and July 1993 (Fig. 3). All the subsequent runs used a biased set of atmospheric forcing, characterized by uniformly drier conditions obtained by multiplying the base run precipitation and evaporation rates by a factor of 0.50 and 1.50, respectively. The open loop scenario simply consisted of a single run (one realization) using biased atmospheric forcings. Observation values from the base run were selected every 6 d at six points distributed across the catchment (Fig. 2) for pressure head and soil moisture and at the catchment outlet cell of the surface DEM for streamflow. At each of the six points, soil moisture values were extracted at the surface node while pressure head measurements were extracted at the two bottom nodes. Initial conditions for all runs were generated with a 10-d simulation during which the catchment, initially fully saturated, was subjected to an evaporative flux of 0.25 mm h$^{-1}$ (6 mm d$^{-1}$). The pressure head distribution thus computed represents

TABLE 1. Soil properties for the Brisy catchment at soil depth increments from 0 to 3.0 m. For the ensemble Kalman filter (EnKF) simulations, parameter values represent the nominal ensemble mean.

| Soil parameter | Value | | | | | |
|---|---|---|---|---|---|---|
| | 0–0.27 m | 0.27–0.63 m | 0.63–1.02 m | 1.02–1.68 m | 1.68–2.34 m | 2.34–3.00 m |
| Saturated conductivity ($K_s$), m h$^{-1}$ | 0.025 | 0.025 | 0.025 | 0.00371 | 0.00371 | 0.00371 |
| Aquifer specific storage ($S_s$), m$^{-1}$ | 0.016 | 0.016 | 0.016 | 0.016 | 0.016 | 0.016 |
| Porosity ($\phi$) | 0.45 | 0.45 | 0.45 | 0.49 | 0.49 | 0.49 |
| van Genuchten (1980) retention curve parameter $\alpha$, m$^{-1}$ | 1.45 | 1.45 | 1.45 | 1.45 | 1.45 | 1.45 |
| van Genuchten (1980) retention curve parameter $n$ | 3.245 | 3.245 | 3.245 | 3.245 | 3.245 | 3.245 |
| Residual moisture content ($\theta_r$) | 0.085 | 0.085 | 0.085 | 0.085 | 0.085 | 0.085 |

the actual initial conditions for the true, the open loop, and the NN runs and the nominal mean values of the initial conditions for all the EnKF runs.

All the parameters relative to the data assimilation runs are summarized in Table 2 and include $G$, $\varepsilon$, and the spatial and temporal weighting functions for NN and the uncertainty, in terms of the CV, used in the definition of the ensemble for the EnKF. The values of $G$ and $\tau_c$ were assigned on the basis of the numerical experiments reported in Hurkmans et al. (2006) and correspond to the best compromise between numerical effort and retrieval potential of the current implementation of the nudging scheme, while the chosen value of $\varepsilon$ reflects the same measurement accuracy adopted for the EnKF. The Gaussian-exponential weighting functions describe the spatial and temporal correlation behavior of the nudging observations and mimic the time behavior of the EnKF. This is probably not an optimal choice for NN compared with the more typical Cressman-type functions (Stauffer and Seaman, 1990) as it does not consider the influence of observations backward in time, but it is consistent with the behavior of our EnKF implementation. We want to stress that the choice of weighting functions in nudging implementations is still an unresolved issue, is often made empirically, and may have a strong influence on the performance of the scheme. For the EnKF runs, as mentioned above, we took into account the uncertainty of the initial conditions, boundary conditions, and the model parameters, generating an ensemble of realizations by perturbing all the aforementioned factors. In these scenarios, the largest uncertainty was assigned to the saturated hydraulic conductivity (CV = 50%, i.e., a standard deviation 0.5 times the nominal values), while a smaller CV was ascribed to the initial conditions (CV = 20%). The rainfall (positive values) and evaporation (negative values) rates shown in Fig. 3 represent the time-variable mean of the atmospheric forcings, perturbed with random lognormal fluctuations with CV = 20% and a time decorrelation length $T$ = 30 h. For both data assimilation techniques, two scenarios were examined: pressure head assimilation (NN-$\psi$ and EnKF-$\psi$) and soil moisture assimilation (NN-$\theta$ and EnKF-$\theta$). For the EnKF, a third scenario with streamflow as the observation variable was also simulated (EnKF-$Q$).

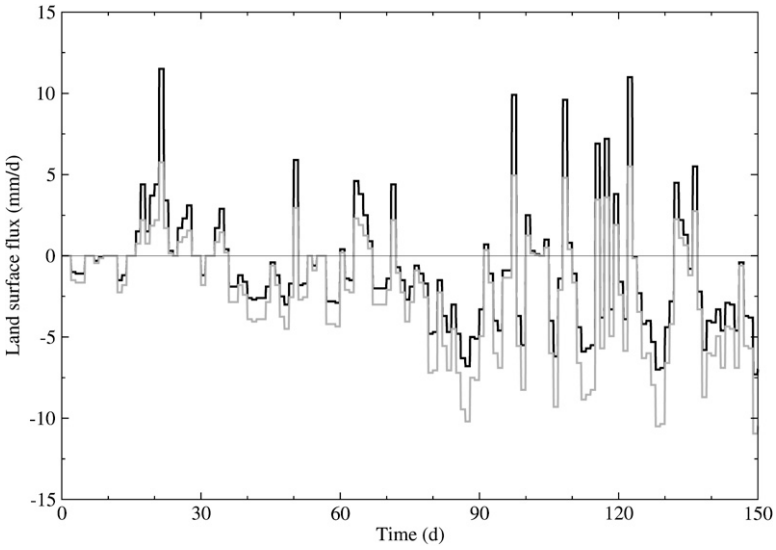


FIG. 3. Net atmospheric boundary conditions for the base run (black) and the open loop and data assimilation runs (gray). The plotted series represents the actual forcing imposed on the Newtonian nudging and open loop scenarios and the nominal mean for the ensemble Kalman filter scenarios. Positive values correspond to rainfall rates and negative values to evaporation rates.

## Numerical Results

Computational performance statistics for all the simulations are summarized in Table 3, which shows the number of backsteps (i.e., nonlinear convergence failures that cause a repetition of the time step with a smaller $\Delta t$), total number of time steps, average time step size, average number of nonlinear iterations per time step, and the total CPU time. As expected, nudging is computationally more efficient than the EnKF, chiefly because the latter needs, in our case, the forward propagation of 100 realizations. The ensemble size was chosen on the basis of previous similar experiments (Camporese et al., 2009b). Note that some realizations may use combinations of parameter values that cause computational difficulties and lead to a drop in the average time step size with respect to the NN runs. As far as NN is concerned, assimilation of pressure head is more computationally demanding than assimilation of soil moisture, due to different strengths of the forcing functions affecting the stiffness of the ordinary differential equation (ODE) system that arises from the spatial discretization of Eq. [3]. We should note that we are using standard backward Euler for the time discretization, so that the stiffness of the ODE system affects the time step size that guarantees convergence of the nonlinear iteration (Gustafsson and Söderlind, 1997). For the EnKF, assimilation of streamflow is more expensive than assimilation of pressure head or soil moisture. This is due to the characteristics of the covariance matrix between the streamflow at the outlet and the pressure head distribution of the watershed, which, as shown by Camporese et al. (2009b), is often badly ill con-

TABLE 2. Nudging and ensemble Kalman filter parameters used in the data assimilation runs. For the ensemble Kalman filter (EnKF) uncertainty levels (CVs) are also indicated.

| Data assimilation method | Parameter |
|---|---|
| Nudging | nudging term relative strength with respect to physical forcing ($G$) = 0.5 $h^{-1}$ (assimilation of surface moisture content, $\theta$) |
| | $G$ = 0.15 $m^{-1}$ $h^{-1}$ (assimilation of bottom layer pressure head, $\psi$) |
| | observation accuracy ($\varepsilon$) = 0.99 |
| | horizontal radius of influence ($R_{xy}$) = 500 m |
| | vertical radius of influence ($R_z$) = 0.5 m |
| | characteristic observation-influenced time window ($\tau_c$) = 6 h |
| Ensemble Kalman filter | ensemble size = 100 |
| | lognormal saturated hydraulic conductivity ($K_s$) (CV = 50%) |
| | lognormal aquifer specific storage coefficient ($S_s$) (CV = 20%) |
| | normal initial conditions (CV = 20%) |
| | lognormal atmospheric forcing (CV = 20%) |
| | lognormal $\theta$ and outlet streamflow ($Q$) measurements (CV = 1.0%) |
| | normal $\psi$ measurements (CV = 1.0%) |
| | atmospheric forcing decorrelation time ($T$) = 30 h |
| All | observation interval = 144 h |

TABLE 3. Summary of numerical results for the base, open loop, and the Newtonian nudging (NN) and ensemble Kalman filter (EnKF) data assimilation runs for surface soil moisture (θ), pressure head at the bottom layer of the catchment (ψ), and streamflow at the catchment outlet (*Q*).

| Parameter | Base run | Open loop | NN-ψ | NN-θ | EnKF-ψ | EnKF-θ | EnKF-*Q* |
|---|---|---|---|---|---|---|---|
| Backsteps | 0 | 0 | 365 | 61 | 345 | 22 | 1,328 |
| No. of time steps | 1,937 | 1,937 | 4,783 | 2,210 | 8,535 | 6,039 | 17,905 |
| Average time step size, h | 1.86 | 1.86 | 0.75 | 1.63 | 0.42† | 0.60† | 0.20† |
| Average nonlinear iterations per time step | 2.29 | 2.66 | 4.43 | 3.42 | 162.77‡ | 188.72‡ | 161.84‡ |
| Total CPU time, s | 561 | 637 | 16,568 | 2750 | 170,609‡ | 138,880‡ | 364,538‡ |

† Ensemble average.
‡ Sum of all the ensemble members.

ditioned. This is reflected in our simulations by the large number of backsteps, small time steps, and hence more CPU effort.

Figure 4 shows the difference in surface saturation between the perturbed atmospheric boundary condition runs (including the open loop) and the base run at the end of the simulation ($t$ = 3600 h), which coincides with the last update. The estimate of the system state for the EnKF runs is represented by the ensemble average. Both NN runs show a spatially limited retrieval capability, accurately recovering the true saturation only in the vicinity of the measurement points, while both scenarios of the EnKF are much more effective and are able to improve surface soil moisture for the whole catchment. This result was not surprising, since the covariance matrices of the EnKF scheme have the capability to take into account the correlation existing between points located far apart across the catchment. Assimilation of θ, for both NN and the EnKF, manifests a slight overshooting effect, probably due to the nonlinearity of the operator $M$, which relates the soil moisture measurements to the subsurface system state (expressed in terms of ψ). This phenomenon is indeed absent when $M$ is linear, as for example in the case when only pressure heads are assimilated. On the other hand, assimilation of ψ seems to be less effective than θ, the latter exhibiting an overall better performance for a given assimilation scheme. We note that the catchment remains relatively wet throughout the simulation, with a generally shallow water table except at the highest elevations. Finally, assimilation of streamflow alone is not able to recover the saturation state of the catchment, resulting in only a minor improvement with respect to the open loop scenario. This is probably due to the aggregated nature of the measurement, along with the limited dimension of the measurement space (equal to 1 in this case) with respect to the system state space (close to 50,000) and, as mentioned above, the ill conditioning of the Kalman gain.

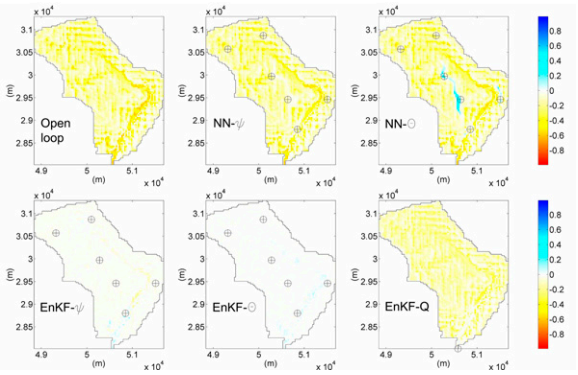


FIG. 4. Difference in water saturation at the surface nodes between the open loop run and the base run and between the base run and the Newtonian nudging (NN) and ensemble Kalman filter (EnKF) data assimilation runs for surface soil moisture (θ), pressure head at the bottom layer of the catchment (ψ), and streamflow at the catchment outlet (*Q*) at the end of the simulation ($t$ = 3600 h) .

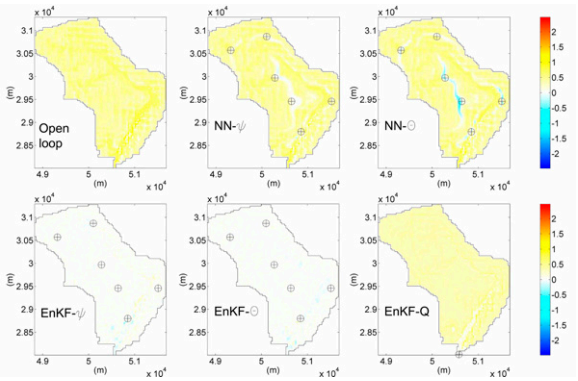


FIG. 5. Difference in water table depth between the open loop run and the base run and between the base run and the Newtonian nudging (NN) and ensemble Kalman filter (EnKF) data assimilation runs for surface soil moisture (θ), pressure head at the bottom layer of the catchment (ψ), and streamflow at the catchment outlet (*Q*) at the end of the simulation ($t$ = 3600 h).

Figure 5 is analogous to Fig. 4 but reports water table depth rather than surface saturation. The results are broadly consistent with those of Fig. 4, with a few notable differences. Similarly to the previous case, the EnKF performed better than NN. The EnKF results for the scenario of streamflow assimilation suffer from the same drawbacks mentioned above. Assimilation of soil moisture exhibits some numerical overshooting, especially for the NN scenario, again probably due to the nonlinearity of the retention curves. Still, assimilation of θ performed slightly better than assimilation of ψ in terms of water table depth for the EnKF scenarios. The water table depth in the case of pressure head assimilation was, in fact, slightly overestimated in the vicinity of the Brisy streambed, where, instead, it was better matched for the scenario of streamflow assimilation. This unexpected behavior may be explained by the smaller variability that characterizes the pressure head in the saturated zone, especially near the bottom layer of the three-dimensional grid, compared with the soil moisture variability at the surface. A larger variability of the system state in fact implies a stronger correction when an update occurs. This explanation, however, cannot be generalized and holds as long as the soil moisture does not get too close to its upper and lower limits, i.e., saturated and irreducible water content, respectively. When soil moisture is near these limits, the covariance matrix approaches identity, and moreover, the distribution of θ would become skewed and thus stray from the hypothesis of a Gaussian distribution that is required for Eq. [7] to yield an optimal update.

The results discussed above find further confirmation in Fig. 6, which shows the time evolution of subsurface storage for all the simulations. The EnKF performed better than NN in retrieving

the overall subsurface response of the catchment except for the case of streamflow assimilation, which yielded results comparable to the two nudging scenarios. Assimilation of soil moisture by the EnKF gave a slightly more accurate estimate of the subsurface volume than the corresponding assimilation of pressure head.

Figure 7 shows the streamflow hydrograph at the catchment outlet (bottom panel) for all the simulations, as well as the cumulated streamflow hydrographs (top panel). Nudging provided a limited contribution to the improvement of the hydrograph, consistent with the results for the subsurface state. Note that the only runoff generation mechanism for this test case was saturation excess. We conclude that NN does not provide sufficient groundwater to fill the catchment subsurface, and thus the runoff component of the watershed response cannot be improved significantly. On the other hand, the EnKF, as implemented in CATHY, also updates the overland flow system even for measurements related to the subsurface alone. This feature, combined with the capability of the EnKF scheme to capture subsurface dynamics, allows the streamflow hydrograph to be improved significantly with respect to the open loop run. Despite the general improvement in terms of cumulated volume, there are still a few mismatches between the true solution and the two EnKF scenarios, as can be seen, for instance, in the delay affecting the first and largest streamflow peak. The timing and peak errors seem to be more significant when not assimilating streamflow. On the other hand, there are significant drawbacks when not assimilating distributed, subsurface state variables such as pressure head or soil moisture. In this case, a closer inspection of Fig. 7 reveals an erratic peak in the EnKF-*Q* streamflow immediately following the updates. This is due again to the ill-conditioned covariance matrix, which causes an overshooting of the surface volume update and hence the subsequent streamflow peak when this volume reaches the outlet.

To conclude our analysis, we show the behavior of the RMSE (m), calculated for the subsurface state as

$$\mathrm{RMSE} = \sqrt{\frac{\sum_{i=1}^{N}\left(\psi_i^{\mathrm{a}} - \psi_i^{\mathrm{t}}\right)^2}{N}} \qquad [9]$$

where $N$ is the number of subsurface grid nodes, $\psi_i^{\mathrm{a}}$ is the pressure head estimate at the $i$th node, and $\psi_i^{\mathrm{t}}$ is the true (base run) pressure head at the $i$th node. The time evolution of the RMSE is shown in Fig. 8 for all the runs, demonstrating that the EnKF consistently outperforms NN in all cases. For the surface state, we calculate the time average of the outlet streamflow square error as follows:

$$\mathrm{RMSE}_Q = \sqrt{\frac{\sum_{i=1}^{N_{\mathrm{t}}}\left(Q_i^{\mathrm{a}} - Q_i^{\mathrm{t}}\right)^2}{N_{\mathrm{t}}}} \qquad [10]$$

where $N_{\mathrm{t}}$ is the number of time steps, $Q_i^{\mathrm{a}}$ is the outlet streamflow estimate at the $i$th time step, and $Q_i^{\mathrm{t}}$ is the true (base run) outlet streamflow at the $i$th time step. The streamflow $\mathrm{RMSE}_Q$ are reported in Table 4 for all scenarios. Again, the EnKF outperforms NN in all cases. Obviously the integral nature of $\mathrm{RMSE}_Q$ does not provide an accurate measure of the instantaneous errors, which is better conveyed in Fig. 7; still, we use Eq. [10] to compare the performances of different schemes. From the table, we observe that the best $\mathrm{RMSE}_Q$ reduction with respect to the open loop was obtained by assimilation of soil moisture and not by assimilation

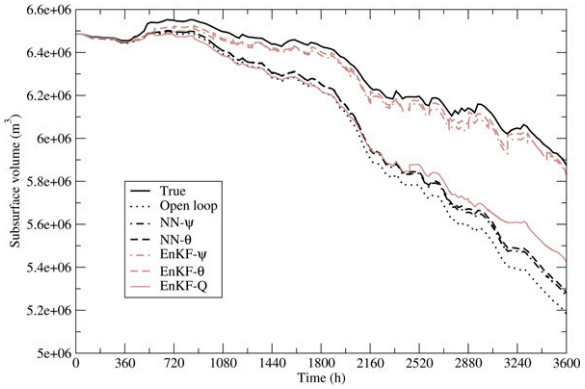


FIG. 6. Time evolution of the water volume stored in the catchment subsurface for the base run, the open loop run, and the Newtonian nudging (NN) and ensemble Kalman filter data assimilation runs for surface soil moisture (θ), pressure head at the bottom layer of the catchment (ψ), and streamflow at the catchment outlet (*Q*). The storage includes both the saturated zone and the vadose zone.

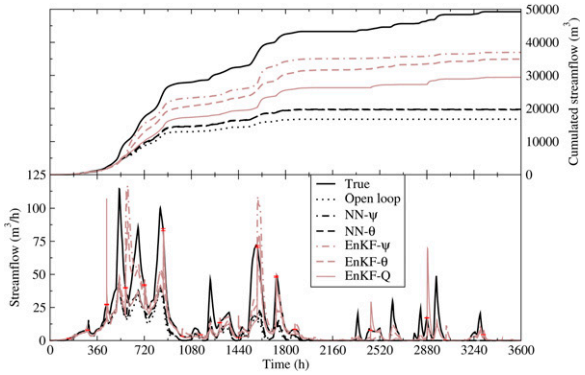


FIG. 7. Streamflow hydrograph (bottom) and cumulated streamflow volume (top) at the catchment outlet for the base run, the open loop run, and Newtonian nudging (NN) and ensemble Kalman filter (EnKF) data assimilation runs for surface soil moisture (θ), pressure head at the bottom layer of the catchment (ψ), and streamflow at the catchment outlet (*Q*). The red symbols denote the streamflow observations used for scenario EnKF-*Q*.

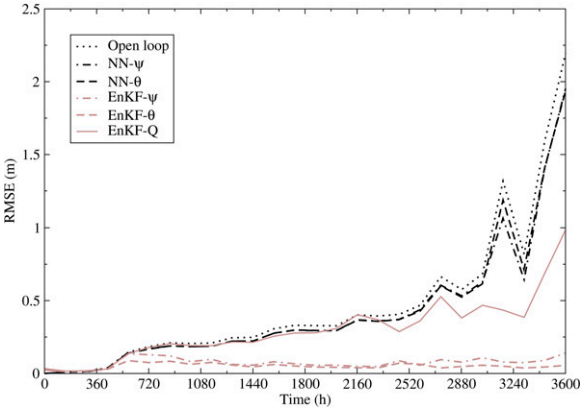


FIG. 8. Time evolution of the RMSE computed on the system state in terms of pressure head across the entire three-dimensional subsurface grid using Eq. [9] for the Newtonian nudging (NN) and ensemble Kalman filter (EnKF) data assimilation runs for surface soil moisture (θ), pressure head at the bottom layer of the catchment (ψ), and streamflow at the catchment outlet (*Q*).

TABLE 4. Outlet streamflow $RMSE_Q$ for the open loop and all assimilation scenarios, and reduction percentage in $RMSE_Q$ relative to the open loop case for the Newtonian nudging (NN) and ensemble Kalman filter (EnKF) data assimilation runs for surface soil moisture ($\theta$), pressure head at the bottom layer of the catchment ($\psi$), and streamflow at the catchment outlet ($Q$).

| Parameter | Open loop | NN-$\psi$ | NN-$\theta$ | EnKF-$\psi$ | EnKF-$\theta$ | EnKF-$Q$ |
|---|---|---|---|---|---|---|
| $RMSE_Q$, $m^3\ s^{-1}$ | 15.92 | 14.71 | 14.78 | 13.59 | 11.74 | 13.45 |
| $RMSE_Q$ reduction, % | – | 7.59 | 7.70 | 15.72 | 30.71 | 21.01 |

of streamflow, another symptom of the ill conditioning that affects the covariance matrices when assimilating only surface discharge.

## Conclusions

Two data assimilation techniques implemented in a detailed, process-based, hydrologic model of coupled surface–subsurface flow were compared for a small catchment test case. The first method, Newtonian relaxation or nudging, was easy to implement and less computationally expensive, but its capability to retrieve the true system state strongly depends on the number of spatial observations. We showed that assimilation of either pressure head or soil moisture can improve the subsurface state only locally, in the vicinity of the measurement locations. As a result, the streamflow hydrograph cannot be accurately recovered without a large number of observations, since subsurface storage is underestimated (for the case of perturbation to drier conditions, as simulated in this study). On the one hand, spurious correlation between points characterized by different dynamics may be introduced if the radius of influence of the nudging term weighting functions is extended over the real physical correlation distance of the system state. On the other hand, increasing the relaxation time $G$ may result in an improved subsurface storage retrieval, but at the cost of a much larger computational effort (Paniconi et al., 2003; Hurkmans et al., 2006) unless more appropriate time integrators are used (Ascher and Petzold, 1998). Moreover, there is an upper limit of $G$ recommended in the literature, equal to $1/\Delta t$ for the case of soil moisture assimilation (Stauffer and Seaman, 1990), that should not be exceeded. A possible approach to improve the performance of NN could be to use the covariance matrix structures obtained from an EnKF application to define new weighting functions in a matrix form. This idea requires careful study of the dynamics of the covariance matrices for this type of hydrologic application, and is left as a possible topic for future research.

The second assimilation method examined, the EnKF, is more computationally expensive but is more effective in retrieving the true system state. Its capability resides in the covariance matrices used by the algorithm, which automatically take into account the physical correlation of the system state values between points located far apart across the domain. Assimilation of both pressure head and soil moisture with the EnKF resulted in an almost complete retrieval of the true subsurface state and in a significant improvement of the streamflow hydrograph. On the other hand, assimilation of streamflow alone at the catchment outlet performed worse than assimilation of $\theta$ and $\psi$, in terms of both the subsurface state and the streamflow hydrograph, mainly due to the ill conditioning of the covariance matrix between streamflow at the outlet and the pressure head distribution. This arises from the aggregated nature of the assimilated variable and causes some numerical artifacts that cannot be easily controlled.


### Acknowledgments

We acknowledge the financial support of the Ouranos Consortium and the Natural Sciences and Engineering Research Council of Canada (Project CRDPJ-319968-04), the University of Padova (Research Fellowship CPDR075551/07), and the Italian Ministry of Education, University, and Scientific Research (PRIN 2007 Projects 200788W4EC and 20074TZWNJ).


## References


Ascher, U.M., and L.R. Petzold. (1998). Computer methods for ordinary differential equations and differential-algebraic equations. Soc. Ind. Appl. Math., Philadelphia.

Aubert, D., C. Loumagne, and L. Oudin. 2003. Sequential assimilation of soil moisture and streamflow data in a conceptual rainfall–runoff model. J. Hydrol. 280:145–161.

Bixio, A.C., S. Orlandini, C. Paniconi, and M. Putti. 2000. Physically-based distributed model for coupled surface runoff and subsurface flow simulation at the catchment scale. p. 1115–1122. *In* Proc. Int. Conf. on Computational Methods in Water Resourc., 13th, Calgary, AB, Canada. 25–29 June 2000. Vol. 2. Balkema, Rotterdam, the Netherlands.

Camporese, M., C. Paniconi, M. Putti, and S. Orlandini. 2009a. Surface–subsurface flow modeling with path-based runoff routing, boundary condition-based coupling, and assimilation of multisource observation data. Waer Resour. Res. (in press) doi:10.1029/2008WR0007536.

Camporese, M., C. Paniconi, M. Putti, and P. Salandin. 2009b. Ensemble Kalman filter data assimilation for a process-based catchment scale model of surface and subsurface flow. Water Resour. Res. (in press), doi:10.1029/2008WR007031.

Chen, F., K. Mitchell, J. Schaake, Y. Xue, H.L. Pan, V. Koren, Q.Y. Duan, M. Ek, and A. Betts. 1996. Modeling of land-surface evaporation by four schemes and comparison with FIFE observations. J. Geophys. Res. 101:7251–7268.

Chen, Y., and D. Zhang. 2006. Data assimilation for transient flow in geologic formations via ensemble Kalman filter. Adv. Water Resour. 29:1107–1122.

Clark, M.P., D.E. Rupp, R.A. Woods, X. Zheng, R.P. Ibbitt, A.G. Slater, J. Schmidt, and M.J. Uddstrom. 2008. Hydrological data assimilation with the ensemble Kalman filter: Use of streamflow observations to update states in a distributed hydrological model. Adv. Water Resour. 31:1309–1324.

Crow, W.T., and E. Van Loon. 2006. Impact of incorrect model error assumptions on the sequential assimilation of remotely sensed surface soil moisture. J. Hydrometeorol. 7:421–432.

Dai, Y., X. Zeng, R.E. Dickinson, I. Baker, G.B. Bonan, M.G. Bosilovich, et al. 2003. The Common Land Model (CLM). Bull. Am. Meteorol. Soc. 84:1013–1023.

Das, N.N., and B.P. Mohanty. 2006. Root zone soil moisture assessment using remote sensing and vadose zone modeling. Vadose Zone J. 5:296–307.

Davies, H.C., and R.E. Turner. 1977. Updating prediction models by dynamical relaxation: An examination of the technique. Q. J. R. Meteorol. Soc. 103:225–245.

De Lannoy, G.J.M., R.H. Reichle, P.R. Houser, V.R.N. Pauwels, and N.E.C. Verhoest. 2007. Correcting for forecast bias in soil moisture assimilation with the ensemble Kalman filter. Water Resour. Res. 43:W09410, doi:10.1029/2006WR005449.

D'Haese, C.M.F., M. Putti, C. Paniconi, and N.E.C. Verhoest. 2007. Assessment of adaptive and heuristic time stepping for variably saturated flow. Int. J. Numer. Methods Fluids 53:1173–1193.

Drécourt, J.-P., H. Madsen, and D. Rosbjerg. 2006a. Bias aware Kalman filters: Comparison and improvements. Adv. Water Resour. 29:707–718.

Drécourt, J.-P., H. Madsen, and D. Rosbjerg. 2006b. Calibration framework for a Kalman filter applied to a groundwater model. Adv. Water Resour. 29:719–734.

Entekhabi, D., H. Nakamura, and E.G. Njoku. 1994. Solving the inverse problem for soil moisture and temperature profiles by sequential assimilation of multifrequency remotely sensed observations. IEEE Trans. Geosci. Remote Sensing 32:438–448.

Evensen, G. 1994. Sequential data assimilation with a nonlinear quasi-geostrophic model using Monte Carlo methods to forecast error statistics. J. Geophys. Res. 99(C5):10143–10162.

Evensen, G. 2003. The Ensemble Kalman Filter: Theoretical formulation and practical implementation. Ocean Dyn. 53:343–367.

Evensen, G. 2006. Data assimilation: The ensemble Kalman filter. Springer, New York.

Georgakakos, K.P. and O.W. Baumer 1996. Measurement and utilization of on-site soil moisture data. J. Hydrol. 184:131–152.

Gustafsson, K., and G. Söderlind. 1997. Control strategies for the iterative solution of nonlinear equations in ODE solvers. SIAM J. Sci. Comput. 18:23–40.

Hantush, M.M., and M.A. Mariño. 1997. Estimation of spatially variable aquifer hy-

draulic properties using Kalman filtering. J. Hydraul. Eng. 123:1027–1035.
Hoeben, R., and P.A. Troch. 2000. Assimilation of active microwave observation data for soil moisture profile estimation. Water Resour. Res. 36:2805–2819.
Houser, P.R., W.J. Shuttleworth, J.S. Famiglietti, H.V. Gupta, K.H. Syed, and D.C. Goodrich. 1998. Integration of soil moisture remote sensing and hydrologic modeling using data assimilation. Water Resour. Res. 34:3405–3420.
Hurkmans, R., C. Paniconi, and P.A. Troch. 2006. Numerical assessment of a dynamical relaxation data assimilation scheme for a catchment hydrological model. Hydrol. Processes 20:549–563.
Kalman, R.E. 1960. A new approach to linear filtering and prediction problems. J. Basic Eng. 82:35–45.
Kollat, J.B., P.M. Reed, and D.M. Rizzo. 2008. Addressing model bias and uncertainty in three-dimensional groundwater transport forecasts for a physical aquifer experiment. Geophys. Res. Lett. 35:L17402, doi:10.1029/2008GL035021.
Kollet, S.J., and R.M. Maxwell. 2006. Integrated surface–groundwater flow modeling: A free-surface overland flow boundary condition in a parallel groundwater flow model. Adv. Water Resour. 29:945–958.
Kollet, S.J., and R.M. Maxwell. 2008a. Capturing the influence of groundwater dynamics on land surface processes using an integrated, distributed watershed model. Water Resour. Res. 44:W02402, doi:10.1029/2007WR006004.
Kollet, S.J., and R.M. Maxwell. 2008b. Demonstrating fractal scaling of base flow residence time distributions using a fully-coupled groundwater and land surface model. Geophys. Res. Lett. 35:L07402, doi:10.1029/2008GL033215.
Koster, R., and M. Suarez. (1996). Energy and water balance calculation in the mosaic LSM. NASA Tech. Mem. 1046069. Vol. 9. Goddard Space Flight Ctr., Greenbelt, MD.
Kosugi, K., S. Katsura, T. Mizuyama, S. Okunaka, and T. Mizutani. 2008. Anomalous behavior of soil mantle groundwater demonstrates the major effects of bedrock groundwater on surface hydrological processes. Water Resour. Res. 44:W01407, doi:10.1029/2006WR005859.
Li, Z., and I.M. Navon. 2001. Optimality of variational data assimilation and its relationship with the Kalman filter and smoother. Q. J. R. Meteorol. Soc. 127B:661–684.
Liang, X., E.F. Wood, and D.P. Lettenmaier. 1996. Surface soil moisture parameterization of the VIC-2L model: Evaluation and modifications. Global Planet. Change 13:195–206.
Liu, G., Y. Chen, and D. Zhang. 2008. Investigation of flow and transport processes at the MADE site using ensemble Kalman filter. Adv. Water Resour. 31:975–986.
Margulis, S.A., D. McLaughlin, D. Entekhabi, and S. Dunne. 2002. Land data assimilation and estimation of soil moisture using measurements from the Southern Great Plains 1997 Field Experiment. Water Resour. Res. 38:1299, doi:10.1029/2001WR001114.
Margulis, S., E. Wood, and P. Troch. 2006. The terrestrial water cycle: Modeling and data assimilation across catchment scales. J. Hydrometeorol. 7:309–311.
McLaughlin, D. 2002. An integrated approach to hydrologic data assimilation: Interpolation, smoothing, and filtering. Adv. Water Resour. 25:1275–1286.
Miguez-Macho, G., G.L. Stenchikov, and A. Robock. 2004. Spectral nudging to eliminate the effects of domain position and geometry in regional climate model simulations. J. Geophys. Res. 109:D13104, doi:10.1029/2003JD004495.
Montgomery, D.R., and E. Foufoula-Georgiou. 1993. Channel network source representation using digital elevation models. Water Resour. Res. 29:3925–3934.
Morita, M., and B.C. Yen. 2002. Modeling of conjunctive two-dimensional surface–three- dimensional subsurface flows. J. Hydraul. Eng. 128:184–200.
Orlandini, S., and R. Rosso. 1996. Diffusion wave modeling of distributed catchment dynamics. J. Hydraul. Eng. 1:103–113.
Panday, S., and P.S. Huyakorn. 2004. A fully coupled physically-based spatially distributed model for evaluating surface/subsurface flow. Adv. Water Resour. 27:361–382.
Paniconi, C., M. Marrocu, M. Putti, and M. Verbunt. 2003. Newtonian nudging for a Richards equation-based distributed hydrological model. Adv. Water Resour. 26:161–178.
Paniconi, C., and M. Putti. 1994. A comparison of Picard and Newton iteration in the numerical solution of multidimensional variably saturated flow problems. Water Resour. Res. 30:3357–3374.
Pauwels, V.R.N., and G.J.M. De Lannoy. 2006. Improvement of modeled soil wetness conditions and turbulent fluxes through the assimilation of observed discharge. J. Hydrometeorol. 7:458–477.
Pauwels, V.R.N., R. Hoeben, N.E.C. Verhoest, and F.P. De Troch. 2001. The importance of the spatial patterns of remotely sensed soil moisture in the improvement of discharge predictions for small-scale basins through data assimilation. J. Hydrol. 251:88–102.
Putti, M., and C. Paniconi. 2004. Time step and stability control for a coupled model of surface and subsurface flow. p. 1391–1402. *In* Proc. Int. Conf. on Computational Methods in Water Resour., 15th, Chapel Hill, NC. 13–17 June 2004. Vol. 2. Elsevier, Amsterdam.
Qu, Y. and Duffy, C. J. 2007. A semidiscrete finite volume formulation for multiprocess watershed simulation. Water Resour. Res. 43:W08419, doi:10.1029/2006WR005752.
Reichle, R.H., and R.D. Koster. 2003. Assessing the impact of horizontal error correlations in background fields on soil moisture estimation. J. Hydrometeorol. 4:1229–1242.
Reichle, R.H., D.B. McLaughlin, and D. Entekhabi. 2002a. Hydrologic data assimilation with the ensemble Kalman filter. Mon. Weather Rev. 130:103–114.
Reichle, R.H., J.P. Walker, R.D. Koster, and P.R. Houser. 2002b. Extended versus ensemble Kalman filtering for land data assimilation. J. Hydrometeorol. 3:728–740.
Rodríguez-Iturbe, I., P. D'Odorico, A. Porporato, and L. Ridolfi. 1999. On the spatial and temporal links between vegetation, climate, and soil moisture. Water Resour. Res. 35:3709–3722.
Shu, Q., M.W. Kemblowsky, and M. McKee. 2005. An application of Ensemble Kalman Filter in integral-balance subsurface modeling. Stochastic Environ. Res. Risk Assess. 19:361–374.
Stauffer, D.R., and N.L. Seaman. 1990. Use of four-dimensional data assimilation in a limited-area mesoscale model: I. Experiments with synoptic-scale data. Mon. Weather Rev. 118:1250–1277.
Stauffer, D.R., and N.L. Seaman. 1994. Multiscale four-dimensional data assimilation. J. Appl. Meteorol. 33:416–434.
VanderKwaak, J.E., and E.A. Sudicky. 2000. Application of a physically-based numerical model of surface and subsurface water flow and solute transport. p. 515–523. *In* Calibration and reliability in groundwater modeling: Coping with uncertainty. ModelCARE'99 Conf., Zurich, Switzerland. 20–23 Sept. 1999. IAHS Press, Wallingford, UK.
Van Geer, F.C., C.B.M. Te Stroet, and Z. Yangxiao. 1991. Using Kalman filtering to improve and quantify the uncertainty of numerical groundwater simulations: 1. The role of system noise and its calibration. Water Resour. Res. 27:1987–1994.
van Genuchten, M.Th. 1980. A closed-form equation for predicting the hydraulic conductivity of unsaturated soils. Soil Sci. Soc. Am. J. 44:892–898.
Vereecken, H., J.A. Huisman, H. Bogena, J. Vanderborght, J.A. Vrugt, and J.W. Hopmans. 2008. On the value of soil moisture measurements in vadose zone hydrology: A review. Water Resour. Res. 44:W00D06, doi:10.1029/2008WR006829.
von Storch, H., H. Langenberg, and F. Feser. 2000. A spectral nudging technique for dynamical downscaling purposes. Mon. Weather Rev. 128:3664–3673.
Waldron, K.M., J. Paegle, and J.D. Horel. 1996. Sensitivity of a spectrally filtered and nudged limited-area model to outer model regions. Mon. Weather Rev. 124:529–547.
Walker, J.P., and P.R. Houser. 2001. A methodology for initializing soil moisture in a global climate model: Assimilation of near-surface soil moisture observations. J. Geophys. Res. 106(D11):11761–11774.
Walker, J.P., G.R. Willgoose, and J.D. Kalma. 2001. One-dimensional soil moisture profile retrieval by assimilation of near-surface observations: A comparison of retrieval algorithms. Adv. Water Resour. 24:631–650.
Weerts, A.H., and G.Y.H. El Serafy. 2006. Particle filtering and ensemble Kalman filtering for state updating with hydrological conceptual rainfall–runoff models. Water Resour. Res. 42:W09403, doi:10.1029/2005WR004093.
Weill, S., E. Mouche, and J. Patin. 2009. A generalized Richards equation for surface/subsurface flow modelling. J. Hydrol. 366:9–20.
Wörman, A., A.I. Packman, L. Marklund, J.W. Harvey, and S.H. Stone. 2007. Fractal topography and subsurface water flows from fluvial bedforms to the continental shield. Geophys. Res. Lett. 34:L07402, doi:10.1029/2007GL029426.